

Comparing different coarse-grained potentials for star polymers

Roberto Menichetti*

Dipartimento di Fisica, Sapienza Università di Roma, P.le Aldo Moro 2, I-00185 Roma, Italy

Andrea Pelissetto†

*Dipartimento di Fisica, Sapienza Università di Roma and INFN,
Sezione di Roma I, P.le Aldo Moro 2, I-00185 Roma, Italy*

We compare different coarse-grained single-blob models for star polymers. We find that phenomenological models inspired by the Daoud-Cotton theory reproduce quite poorly the thermodynamics of these systems, even if the potential is assumed to be density dependent, as done in the analysis of experimental results. Using the numerically determined coarse-grained potential, we also determine the minimum value f_c of the functionality of the star polymer for which a fluid-solid transition occurs. By applying the Hansen-Verlet criterion we find $35 < f_c \lesssim 40$. This result is confirmed by an analysis that uses the modified (reference) hypernetted chain method and is qualitatively consistent with previous work.

PACS numbers: 61.25.he, 82.35.Lr

I. INTRODUCTION

Soft materials are physical systems of great interest because of their many applications. Star polymers, obtained by tethering f polymer chains to a central microscopic core, represent a very interesting example. Indeed, by changing the functionality f , one can interpolate between linear chains ($f = 1, 2$) and colloidal spheres, corresponding to $f \gg 1$. Moreover, their particular nature is responsible for the appearance of many static and dynamic peculiar features which are not observed in suspensions of hard-sphere colloids or of linear chains.^{1,2} Full-monomer simulations of star polymers are very difficult because of the complexity of the structure of these molecules and of the large number of monomers involved. Thus, coarse-grained (CG) models, in which each polymer is represented by a single monoatomic molecule — sometimes it is called blob — have been widely used.³ To obtain a faithful representation of the star-polymer solution thermodynamics one should consider n -body interactions among the CG molecules.^{4–6} A considerable simplification occurs if one only considers the dilute regime in which the polymer packing fraction $\Phi = 4\pi R_g^3 N / (3V)$ (here R_g is the zero-density radius of gyration, while N is the number of star polymers in the volume V) is at most of order 1. Indeed, in this case, overlaps are rare and the contributions due to the n -body potentials are small. Hence, a reasonable approximation is obtained by only considering the pair potential between the CG molecules, which is defined as

$$\beta V(r; f) = -\ln \langle e^{-\beta U_{\text{int}}} \rangle_r, \quad (1)$$

where the average is over all pairs of isolated star polymers such that the distance between their centers is r ; U_{int} is the total intermolecular energy. Standard renormalization-group arguments indicate that, if one considers stars made of fL monomers, the adimensional potential $\beta V(r; f)$ is a universal function of $b = r/R_g$

in the limit $L \rightarrow \infty$. Universality implies that, for any given f , the limiting function $\beta V(b; f)$ is independent of the microscopic model. The first studies of star polymer solutions at finite density based on CG models⁷ used phenomenological potentials that were inspired by the Daoud-Cotton model.⁸ They diverged logarithmically as $b \rightarrow 0$, as predicted theoretically,⁹ and showed an exponential (Yukawa) decrease for $b \rightarrow \infty$. Such a large-distance behavior is consistent with the Daoud-Cotton model predictions and was somewhat confirmed by the results of Ref. 10, which found their experimental data to be consistent with an effective interaction decaying as $e^{-\alpha r}$. Such a behavior was also confirmed—albeit with quite large errors—by numerical simulations¹¹ of systems with $f \leq 50$. Subsequent numerical work—but again arms were quite short—did not confirm the Yukawa behavior for $f \leq 18$.¹² This is not surprising, since the Daoud-Cotton model⁸ does not apply for small values of f . Hence, the phenomenological potential of Ref. 7 cannot be used for star polymers with a small number of arms. For these reasons, Ref. 13 suggested that the potential of Ref. 7 should only be used for $f \geq 10$. For smaller values of f , a second phenomenological potential was proposed.¹³ It has the correct logarithmic short-distance behavior and shows a Gaussian large-distance decay, in agreement with the renormalization-group predictions obtained for linear chains ($f = 2$).¹⁴ A direct numerical determination of the universal pair potential $\beta V(b; f)$ was undertaken by Hsu and Grassberger (HG).¹⁵ By means of a large-scale simulation of an optimal model (the Domb-Joyce model¹⁶ at a specific value of the interaction parameter) they obtained accurate estimates of the pair potential for several values of f in the range $2 \leq f \leq 35$ and provided an accurate parametrization of their results which satisfied all theoretical constraints. They checked the predicted logarithmic divergence for small distances⁹ and found a purely Gaussian large-distance decay for all values of f investigated. In particular, while at short distances their numerical po-

tential was close to the potential proposed in Ref. 13, significant differences were observed at large distances, as a consequence of the different (Yukawa vs Gaussian) decay.

The phenomenological potentials introduced in Refs. 7, 13 have been extensively used to study the phase diagram of star polymers,^{17–19} binary star polymer systems,²⁰ mixtures of star polymers and colloids²¹ and of star and linear polymers,^{22,23} and structural arrest in dense star polymer systems.^{24,25} Since they are quite different from the exact one derived by HG,¹⁵ one may question the quantitative and/or qualitative validity of the results obtained. It is thus worthwhile to repeat these calculations by using all CG models, comparing the results obtained by using the phenomenological potentials with those obtained by using the accurate expression of the pair potential obtained by HG,¹⁵ which we take as reference potential.

In this paper, we study the thermodynamic behavior of dilute star-polymer solutions, by using the CG model based on the HG accurate pair potential. We determine the first virial coefficients, the pressure in the dilute regime, and the intermolecular structure factor which is needed to compare the theoretical results with the experimental ones obtained in scattering experiments. These results are then compared with the analogous ones obtained by using the phenomenological potentials of Refs. 7,13. Finally, we investigate the phase diagram of star polymer solutions, identifying the range of values of f for which a liquid-solid transition occurs, again using the HG pair potential.

The paper is organized as follows. In Sec. II we introduce the three different CG models. In Sec. III we discuss the thermodynamical behavior: first, we compute the second and third virial coefficient for each CG model, then the compressibility factor and the intermolecular structure factor. In Sec. IIID we also discuss an extension of the model of Ref. 13, which uses a density dependent corona diameter. Finally, in Sec. IV we discuss the phase diagram and in Sec. V we present our conclusions.

II. THE EFFECTIVE PAIR POTENTIALS: DEFINITIONS

The universal pair potential $\beta\mathcal{V}(b; f)$ was determined numerically in Ref. 15 for several values of f between 2 and 35. The final results were parametrized as

$$\beta\mathcal{V}_{HG}(b; f) = \frac{1}{\tau_f} \ln \left[e^{\tau_f V_{WP}(b) - d_f b^2} + e^{\tau_f V_G(b)} \right], \quad (2)$$

$$V_{WP}(b) = b_f \ln(a_f/b) \quad V_G(b) = c_f e^{-d_f b^2}. \quad (3)$$

The potential depends on five constants a_f , b_f , c_f , d_f , τ_f which are reported in Ref. 15. For $b \rightarrow 0$, $\mathcal{V}(b; f)$ diverges^{9,26} as $\ln 1/b$ with a prefactor that can be expressed in terms of the partition-function exponents γ_f ,

which are known with good precision.²⁷ Parametrization (2) satisfies this property, $\beta\mathcal{V}_{HG}(b; f) \approx b_f \ln(a_f/b)$, the coefficient b_f being equal to the theoretically predicted value. For $b \rightarrow \infty$ the potential behaves as $c_f e^{-d_f b^2}$, where d_f varies between 0.405 ($f = 2$) and 0.68 ($f = 35$).

Numerical studies of the properties of star polymers have often relied on phenomenological expressions for the pair potential. In Ref. 7 the following potential was proposed:

$$\begin{aligned} \beta\mathcal{V}_1(R; f) &= \frac{5f^{3/2}}{18} (-\ln R + K_f) & R \leq 1, \\ &= \frac{5f^{3/2}}{18} \frac{K_f e^{-\sqrt{f}(R-1)/2}}{R} & R > 1, \end{aligned} \quad (4)$$

where $K_f = 1/(1 + \sqrt{f}/2)$, $R = r/\sigma$, and σ is the so-called corona diameter. For $R \rightarrow 0$ the potential shows the expected logarithmic behavior $\hat{b}_f \ln 1/R$ with $\hat{b}_f = 5f^{3/2}/18$. The coefficient \hat{b}_f can be compared with the theoretical result b_f obtained by using the accurate estimates of the partition-function exponents γ_f .²⁷ We obtain $b_f = 2.42(1), 9.90(3), 57.3(6)$ for $f = 4, 10, 30$, to be compared with $\hat{b}_f = 2.22, 8.78, 45.6$ for the same values of f . Differences increase with f and range from 8% for $f = 4$ to 20% for $f = 30$. They are, however, expected to be largely irrelevant for the thermodynamics in the dilute regime, in which overlaps are rare. For $R \rightarrow \infty$ the potential behaves as $e^{-\sqrt{f}R/2}/R$, which is quite different from the behavior observed in numerical simulations (at least for $f \leq 35$), see Eq. (2).

Potential (4) is expected to be reliable only for large values of f , for $f > 10$, say, i.e. in the regime to which the Daoud-Cotton model⁸ applies. For small values of f a different potential was postulated:¹³

$$\begin{aligned} \beta\mathcal{V}_2(R; f) &= \frac{5f^{3/2}}{18} \left(-\ln R + \frac{1}{2\tau^2} \right) & R \leq 1, \\ &= \frac{5f^{3/2}}{36\tau^2} e^{-\tau^2(R^2-1)} & R > 1, \end{aligned} \quad (5)$$

where again $R = r/\sigma$. The adimensional parameter τ determines the large- r behavior of the potential and was determined only for $f = 2$ and $f = 5$: $\tau = 1.03$ and $\tau = 1.12$ in the two cases.

In the following we will compare the predictions of the three CG models defined above: model MHG based on the exact pair potential (2) and models M1 and M2 based on potentials (4) and (5), respectively.

III. RESULTS: STRUCTURE AND THERMODYNAMICS

A. Zero-density results

Knowledge of the pair potential $\mathcal{V}(b; f)$ allows us to compute the universal combination $A_2 = B_2/R_g^3$, where

TABLE I: In the second, third, and fourth column we report virial coefficient ratios computed by using potential $\mathcal{V}_{HG}(b; f)$ (HG). In the last three columns we report literature values obtained from full-monomer (FM) simulations: *a* refers to Ref. 28, *b* to Ref. 29, *c* to Ref. 30, *d* to Ref. 31, *e* to Ref. 32. For a review of older estimates of A_2 , see Ref. 33.

f	$A_2(\text{HG})$	$A_3(\text{HG})$	$g(\text{HG})$	$A_2(\text{FM})$	$A_3(\text{FM})$	$g(\text{FM})$
2	5.51	4.97	0.164	5.500(3) ^a	9.80(2) ^a	0.324(1) ^a
4	10.04	31.8	0.316	9.979(9) ^b	39.56(16) ^b	0.397(2) ^b
5	12.25	54.5	0.363			
6	14.66	85.6	0.398	14.174(16) ^b	90.1(0.4) ^b	0.449(2) ^b
10	20.62	204	0.479			
12	23.97	288	0.501	23.5(2) ^c		
18	29.60	473	0.540	29.6(2) ^c		0.547(5) ^d
						0.58 ^e
24	36.06	721	0.557	34.21(10) ^d	661(6) ^d	0.564(4) ^d
30	38.32	831	0.565	37.65(6) ^d	813(7) ^d	0.574(6) ^d

the second virial coefficient B_2 is defined by the expansion of the (osmotic) pressure Π ,

$$\frac{\Pi}{k_B T \rho} = 1 + B_2 \rho + B_3 \rho^2 + O(\rho^3), \quad (6)$$

in powers of the concentration $\rho = N/V$. Indeed, A_2 is related to the pair potential by the exact relation

$$A_2(f) = 2\pi \int_0^\infty db b^2 \left(1 - e^{-\beta \mathcal{V}(b; f)}\right). \quad (7)$$

In Table I we report the estimates of A_2 for several values of f obtained by using potential (2). If we compare these results with those obtained in the literature from different full-monomer simulations [column $A_2(\text{FM})$] we observe reasonable agreement (the largest deviation, 6.5%, is observed for $f = 24$), confirming the adequacy of parametrization (2) for all values of f .

Using model MHG we can also compute the universal combinations $A_3 = B_3 R_g^{-6}$ and $g = B_3/B_2^2 = A_3/A_2^2$, involving the third virial coefficient B_3 . Since three-body interactions are neglected in the CG model, these estimates differ from those that would be obtained in the exact, full-monomer polymer model. Therefore, the observed discrepancies give us quantitative indications of the role of the neglected many-body interactions in CG single-blob star-polymer models. The results reported in Table I show that many-body forces apparently become less relevant as f increases. For instance, if we consider the relative deviation $\Delta g = 1 - g(\text{HG})/g(\text{FM})$ for the g parameter, we find a very large discrepancy for $f = 2$, $\Delta g \approx 50\%$, but only $\Delta g \approx 11\%$ for $f = 6$. For $f \gtrsim 18$, the CG model apparently reproduces the full-monomer results. This is particularly encouraging since it implies that CG models provide increasingly better approximations as f increases, i.e. exactly in the regime in which full-monomer simulations become unfeasible.

TABLE II: Estimates of σ/R_g , A_2 , and A_3 for models M1 and M2.

f	M1			M2		
	$\sigma/R_g(\text{M1})$	$A_3(\text{M1})$	$g(\text{M1})$	$\sigma/R_g(\text{M2})$	$A_3(\text{M2})$	$g(\text{M2})$
2	0.807	2.01	0.067	1.333	6.35	0.209
4	0.894	16.4	0.163			
5	0.933	30.6	0.204	1.349	61.9	0.412
6	0.974	50.9	0.237			
10	1.062	141	0.332			
18	1.195	376	0.429			
30	1.328	722	0.492			

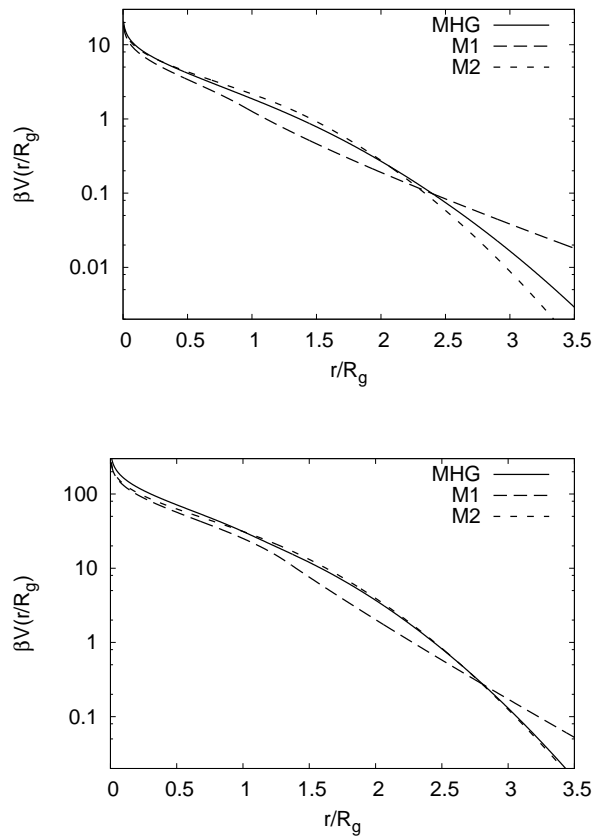


FIG. 1: Comparison of the CG potentials of models MHG, M1, and M2: (top) $f = 5$; (bottom) $f = 30$. For $f = 30$ we fix $\tau = 1$ in model M2 (see Sec. III C).

Let us now perform the same analysis for models M1 and M2. Since the potentials $\mathcal{V}_1(r; f)$ and $\mathcal{V}_2(r; f)$ depend on the corona diameter σ , to obtain quantitative predictions we must determine the ratio σ/R_g . As already suggested in Ref. 21, we fix σ/R_g so that all potentials give the correct result for the second-virial combination A_2 . This guarantees that models M1 and M2 have the correct thermodynamic behavior as $\Phi \rightarrow 0$. Using the estimates of A_2 reported in Table I [column $A_2(\text{HG})$]

we obtain the estimates of σ/R_g reported in Table II. For $f = 18$, Ref. 7 obtained $\sigma/R_g \approx 1.26$ from the analysis of the experimental data, while numerical simulations¹¹ indicate that $\sigma/R_g \approx 1.3$ is a good approximation for model M1 at least for f large. Our numerical results are fully consistent with this approximation. As long as f is larger than 10, the expected range of validity of model M1, $\sigma/R_g \approx 1.3$ holds with a relative error of at most 20%. Such an approximation also holds for model M2 for the two values of f we consider. In the following, we consider models M1 and M2 using the values of σ/R_g reported in Table II. Hence, by construction, all models (M1, M2, and MHG) have the same thermodynamic behavior for $\Phi \rightarrow 0$. In Fig. 1 we compare the different potentials for $f = 5$ and $f = 30$. For $f = 5$ potentials M2 and MHG are very close in the whole interesting range $b = r/R_g \lesssim 2.5$. For larger values, potential M2 decreases slightly faster: $\beta\mathcal{V}_{HG}$ decays as $1.76e^{-0.53b^2}$, while $\beta\mathcal{V}_{M2}$ decays as $4.34e^{-0.69b^2}$. Significant differences are instead observed for potential M1, both for small values of b — it underestimates $\beta\mathcal{V}_{HG}$ — and for large values of b , where it decays slower. Similar discrepancies are observed for $f = 30$.

Let us now compare the third-virial coefficient combinations A_3 and g , see Tables I and II. For model M1, discrepancies are quite large for f small, confirming the inadequacy of the parametrization for these values of f . For $f > 10$ discrepancies are smaller, but still not negligible. For $f = 18$ $g(\text{M1})$ differs from $g(\text{HG})$ and $g(\text{FM})$ by 21%. For $f = 30$ the discrepancy decreases to 13%. For $f \leq 10$ model M2 should be used. Also in this case, we observe significant discrepancies from the results obtained by using the MHG model, but, at least for $f = 2$, model M2 appears to provide a better approximation to the full-monomer results.

B. Integral-equation methods

In order to study the finite-density behavior we used integral-equation methods.³⁴ As usual in these approaches we considered the pair distribution function $g(\mathbf{r})$, the corresponding correlation function $h(\mathbf{r}) = g(\mathbf{r}) - 1$, and the direct correlation function $c(\mathbf{r})$ defined by the Ornstein-Zernike relation³⁴

$$h(\mathbf{r}) = c(\mathbf{r}) + \rho \int d^3\mathbf{s} c(\mathbf{s}) h(\mathbf{r} - \mathbf{s}). \quad (8)$$

This equation must be supplemented by a closure relation. Three different closures were used to check the accuracy of the results. We first used the hypernetted chain (HNC) equation³⁴

$$g(\mathbf{r}) = e^{-\beta V(\mathbf{r}) + h(\mathbf{r}) - c(\mathbf{r})}, \quad (9)$$

which is known to be quite accurate for soft interactions. In our case potentials diverge as $r \rightarrow 0$, hence a better

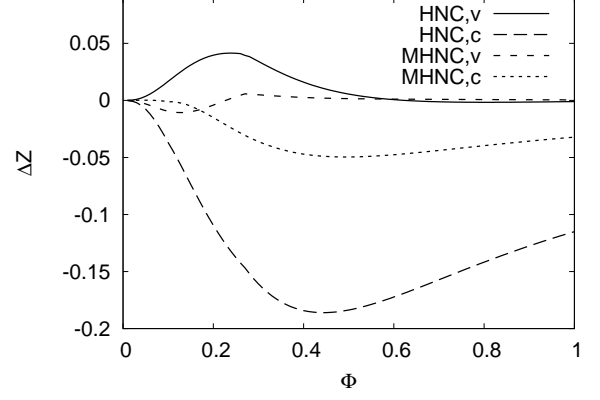


FIG. 2: Relative deviations $\Delta Z_{HNC} = Z_{HNC}/Z_{RY} - 1$ and $\Delta Z_{MHNC} = Z_{MHNC}/Z_{RY} - 1$ for $f = 30$ and model MHG. The virial route (HNC,v and MHNC,v) and the compressibility route (HNC,c and MHNC,c) have been used.

approximation should be provided by the Rogers-Young (RY) closure:³⁵

$$g(\mathbf{r}) = e^{-\beta V(\mathbf{r})} \left\{ 1 + \frac{1}{f(r)} \left[e^{(h(\mathbf{r}) - c(\mathbf{r}))f(r)} - 1 \right] \right\}, \quad (10)$$

with

$$f(r) = 1 - e^{-\alpha r}. \quad (11)$$

The consistency parameter α was redetermined at each density by requiring the equality of the compressibility computed by using $g(\mathbf{r})$ (compressibility route) and that computed by using the virial pressure. This was done iteratively until the relative difference between the two quantities was less than 0.1%. We found that αR_g increases with Φ , varying between 0.5 and 2-2.5 as Φ increases from 0.3 to 1.

For $f \geq 30$ — in this case the potential has a quite hard core — we also used the reference or modified HNC (MHNC) method.^{34,36} The closure relation is written as

$$g(\mathbf{r}) = e^{-\beta V(\mathbf{r}) + h(\mathbf{r}) - c(\mathbf{r}) + E(\mathbf{r})}, \quad (12)$$

where $E(\mathbf{r})$ is the bridge function. For $E(\mathbf{r})$ we used the bridge function of a system of hard spheres of diameter d at the same density (it can be computed quite precisely by using the results reported in Refs. 37,38). The diameter d , or equivalently the hard-sphere packing fraction $\eta_{HS} = \pi d^3 \rho / 6$, was determined by using the Lado criterion,³⁹ which is a way to implement thermodynamic consistency between the virial and the energy route:

$$\int d^3\mathbf{r} [g(\mathbf{r}) - g_{HS}(\mathbf{r}; \eta_{HS})] \frac{\partial E(\mathbf{r}; \eta_{HS})}{\partial \eta_{HS}} = 0. \quad (13)$$

To check the accuracy of the results we computed the compressibility factor

$$Z = \frac{P}{k_B T \rho} \quad (14)$$

for model MHG by using the HNC and the RY closure; for $f \geq 30$ also the MHNC closure was used. As an example, in Fig. 2 we show $\Delta Z_{HNC} = Z_{HNC}/Z_{RY} - 1$ and $\Delta Z_{MHNC} = Z_{MHNC}/Z_{RY} - 1$, where Z_{HNC} , Z_{RY} , and Z_{MHNC} are the compressibility factors computed by using the three different methods. Here we take $f = 30$ and use potential MHG. For the HNC closure, we observe a significant difference between the pressure computed by using the virial and the compressibility route, which however decreases as Φ increases. For the MHNC closure, results are much more consistent, the difference being at most 5%, again decreasing as Φ becomes large. The HNC and MHNC virial pressure differ only slightly from the RY result. If the compressibility route is used, differences are larger. They however decrease as the density increases. The somewhat large difference between the two thermodynamic routes observed for the HNC method is due to the somewhat hard core of the potential, that diverges as $r \rightarrow 0$. It is smaller for smaller values of f : for $f = 6$ and 18, $Z_{HNC,c}$ and $Z_{HNC,v}$ differ at most by 2.2% and 14%, respectively. In all cases the RY closure appears to be reliable, with an error that is probably of the order of a few percent and that decreases as Φ increases.

The results we will present in the following have been obtained by using the RY closure. We will use again the MHNC closure in Sec. IV, where we will discuss the fluid-solid transition in star-polymer solutions.

C. Comparing the potentials at finite density

Let us now discuss the behavior of the different models at finite density in the dilute regime $\Phi \lesssim 1$. Let us first consider the compressibility factor Z . In Fig. 3 we report the relative deviations $\Delta Z = Z/Z_{HG} - 1$, where Z is computed in models M1 and M2, and Z_{HG} is computed in model MHG. As should be expected on the basis of the results for A_3 and g , model M1 underestimates the true CG compressibility factor Z_{HG} . For $\Phi = 1$, we find deviations $\Delta Z = -24\%$, -31% , -32% for $f = 10, 18, 30$, which are quite significant. Model M2 instead overestimates Z_{HG} . Differences are, however, significantly smaller: for $\Phi = 1$, we find $\Delta Z = 2\%$, 6% for $f = 2, 5$.

Since model M2 has the observed Gaussian decay and appears to be relatively accurate, we tried to check whether it is possible to extend it to other values of f , beside $f = 2, 5$. For this purpose we should fix both σ/R_g and τ . If we require $g(M2) \approx g(HG)$ beside $A_2(M2) \approx A_2(HG)$, we obtain $\tau \approx 1$ for all values of f in the range $10 \leq f \leq 35$. The ratio σ/R_g is always consistent with 1.2. More precisely, for $\tau = 1$, we have $\sigma/R_g = 1.203, 1.202$ for $f = 18, 30$, respectively. The corresponding M2 potential has a large-distance behavior which is consistent with that of potential (2). Indeed, we have $\beta V_2(R; f) \sim e^{-0.69b^2}$ for large $b = r/R_g$ to be compared with $\beta V_{HG}(b; f) \sim e^{-d_f b^2}$, $d_f = 0.65, 0.68$ for

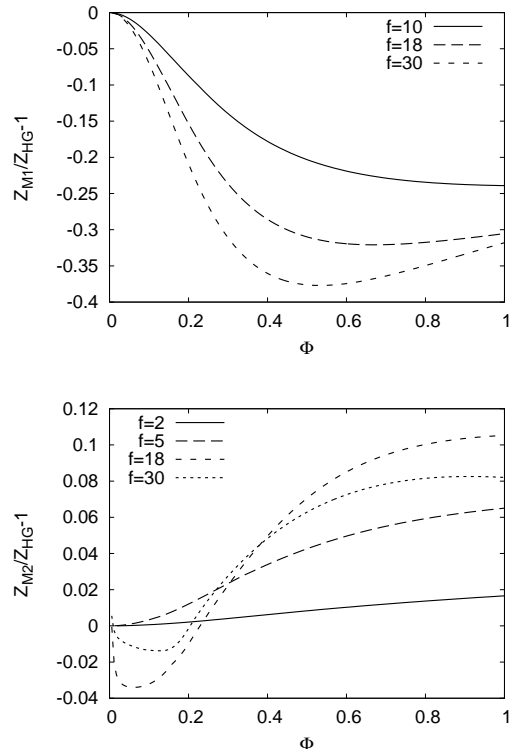


FIG. 3: Relative deviation $\Delta Z = Z/Z_{HG} - 1$ for model M1 ($f = 10, 18, 30$) (top) and model M2 ($f = 2, 5, 18, 30$) (bottom) as a function of the polymer volume fraction Φ . Z_{HG} is the compressibility factor obtained by using potential (2).

$f = 18, 30$, respectively. Potential $\beta V_2(R; f)$ is compared with $\beta V_{HG}(b; f)$ in Fig. 1. On the scale of the figure, no significant differences are observed, confirming that model M2 is a better approximation to the star-polymer CG potential than model M1. In Fig. 3 we also report ΔZ for model M2 with $\tau = 1$ and $f = 18, 30$. Again model M2 overestimates Z_{HG} , but differences are only of order 10% at most.

D. Effective potentials with density-dependent corona diameter

Potential (4) was validated by comparing the theoretical predictions with experimental data for the total scattering intensity $I(q)$. In the dilute regime, $I(q)$ can be factorized⁴⁰ as $I(q) \approx P(q)S(q)$, where $P(q)$ is the single-polymer form factor and $S(q)$ is the intermolecular center-of-mass structure factor, which can be computed by using the three different CG models. In the CG model, $S(q)$ can be obtained as $S(q) = 1 + \rho \hat{h}(q)$, where $\hat{h}(q)$ is the Fourier transform of the correlation function, which is obtained directly in the integral-equation calculation.

Results for $\Phi = 1$ are reported in Fig. 4 for $f = 2, 5, 18, 30$. The results obtained by using model M2 are quite similar to those obtained by using model MHG,

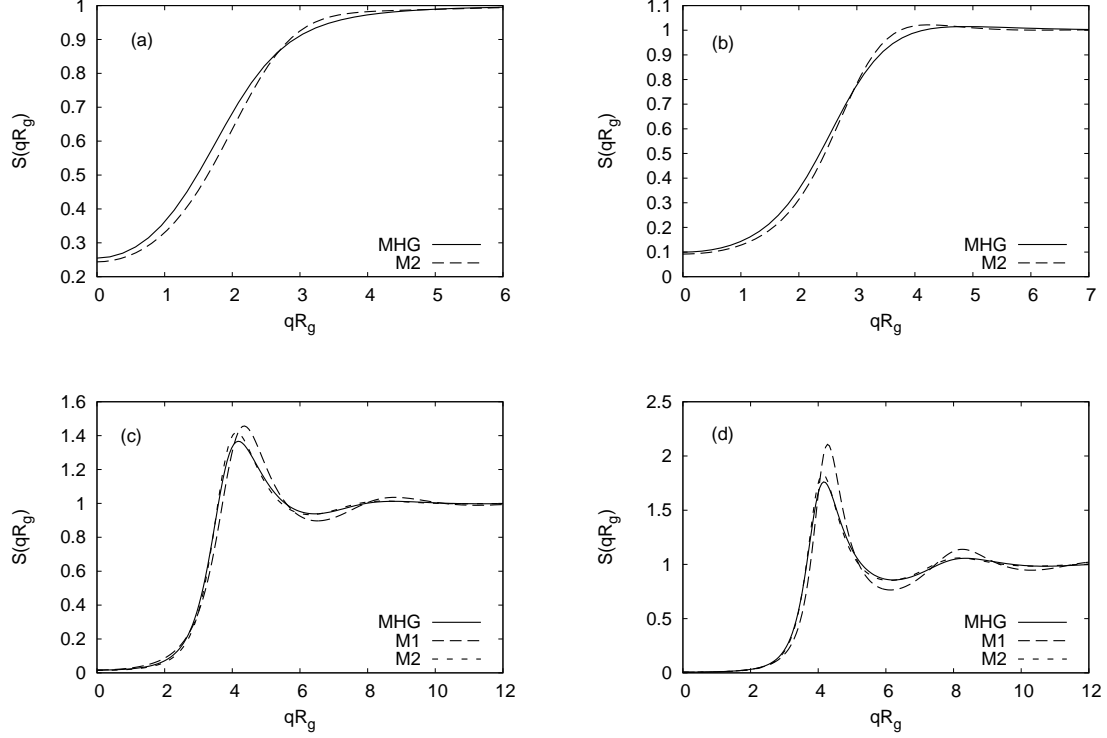


FIG. 4: Structure factor as a function of qR_g for $\Phi = 1$: a) $f = 2$ (models M2, MHG); b) $f = 5$ (models M2, MHG); c) $f = 18$ (models M1, M2, MHG); d) $f = 30$ (models M1, M2, MHG); For $f = 18, 30$ the results for model M2 are obtained by setting $\tau = 1$.

both for $f = 2, 5$, which belong to the original validity range of the potential, and for $f = 18, 30$ (we take $\tau = 1$ in this case). On the other hand, results for model M1 differ significantly. The positions of the minima and maxima are the same for all potentials—not surprising since they are fixed by the dimensions of the polymer—but potential \mathcal{V}_1 gives rise to significantly stronger oscillations for $f \geq 18$.

The results presented here for model M1 are in apparent contradiction with the existing literature. Indeed, potential (4) has been extensively used to analyze experimental data, finding in all cases very good agreement. However, it should be noted that in all these comparisons a density-dependent corona diameter is assumed. For instance, in the original paper⁷ dealing with 18-arm polyisoprene in methylcyclohexane, σ is fixed by $\sigma(\Phi) = 1.26R_g(\Phi)$, where $R_g(\Phi)$ is the density-dependent radius of gyration. A careful study of the density dependence of the corona diameter is presented in Ref. 41 using 57-arm polybutadiene. They find (see the inset of their Fig. 1) that $\sigma(\Phi)$ decreases as Φ increases and that it behaves as $\Phi^{-1/8}$ for $\Phi \gtrsim 1$, in agreement with the density scaling predicted by the Daoud-Cotton model.⁸ Potential (4) has also been validated by using block-copolymer micelles with $f = 63$.¹⁹ However, as in previous cases, a density-dependent corona diameter is assumed.

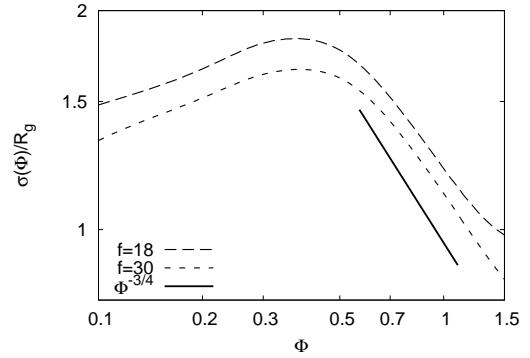


FIG. 5: Log-log plot of the density-dependent corona diameter $\sigma(\Phi)/R_g$ for $f = 18$ and $f = 30$. The solid line corresponds to a behavior $\Phi^{-3/4}$.

To understand the role of a density-dependent corona diameter, we repeat the same analysis as done in experimental work. We take the MHG structure factor as the reference one and determine a density-dependent $\sigma(\Phi)$ such that the M1 structure factor reproduces the MHG one at the same value of Φ . Since the main difference between the MHG and M1 structure factors is the height of the peaks, see Fig. 4, we fix $\sigma(\Phi)$ by requiring that the peak for the lowest value of q has the same height

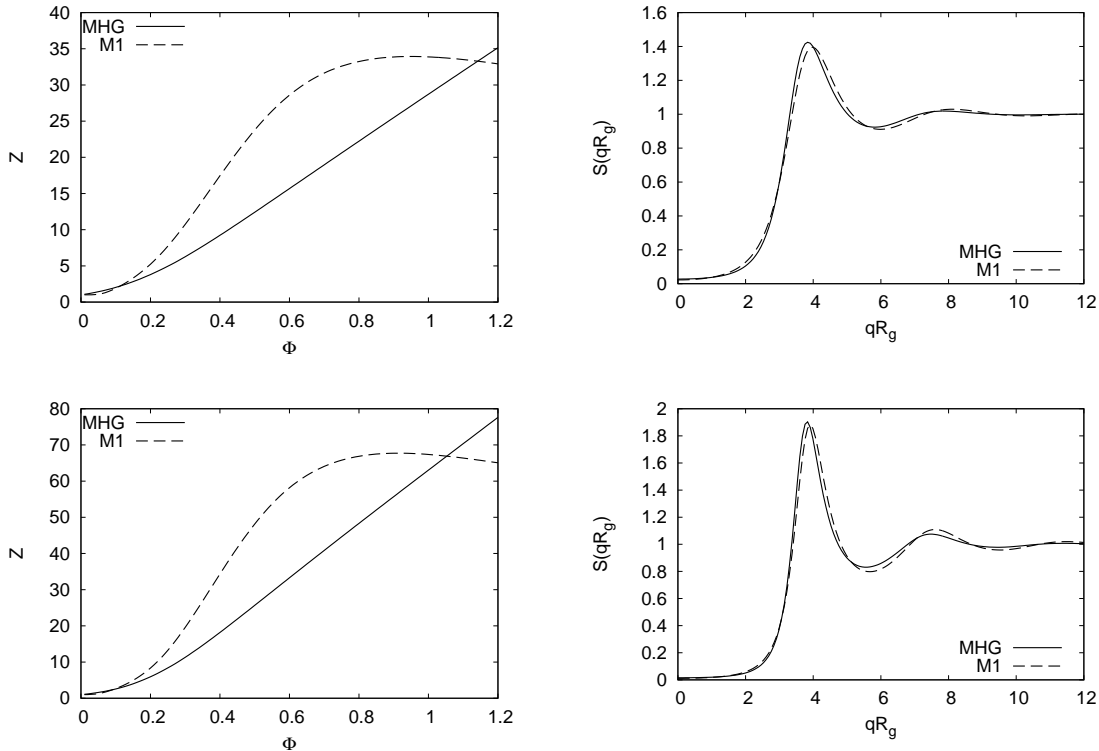


FIG. 6: Compressibility factor Z as a function of Φ (left) and structure factors as a function of qR_g for $\Phi = 1$ (right). Data for model M1 with the density-dependent corona diameter reported in Fig. 5 and for model MHG. Top: $f = 18$; bottom: $f = 30$.

in both models. The results for $f = 18$ and $f = 30$ are reported in Fig. 5. In both cases, $\sigma(\Phi)$ increases for $\Phi \lesssim 0.5$, then shows a maximum at a value which is significantly larger than that obtained by matching the second virial coefficients, and finally decreases. The behavior looks similar to that observed in Ref. 41 (see their Fig. 1). It is also roughly consistent with the predictions of the Daoud-Cotton model, which predicts an intermediate regime in which $\sigma(\Phi) \sim \Phi^{-3/4}$ before the onset of the large- Φ regime where $\sigma(\Phi) \sim \Phi^{-1/8}$. Model M1 with corona diameter $\sigma(\Phi)$ well reproduces the MHG structure factor, as can be seen from Fig. 6.

The computation of the pressure in the presence of a density-dependent potential requires particular care.⁴² We use the HNC closure (thermodynamic consistency does not hold, hence we cannot implement the RY approach) and the compressibility route (the virial route does not provide the correct result, see Ref. 42). The results are shown in Fig. 6. It is evident that Z for model M1 is quite different from that of model MHG. But, even worse, the M1 predicted compressibility factor shows an unphysical decrease for $\Phi \gtrsim 1$, a consequence of the quite rapid decrease of $\sigma(\Phi)$. Clearly, use of a density-dependent corona diameter worsens the thermodynamic behavior of the model.

It is not surprising that $S(q)$ is well reproduced while large differences are observed for Z . Indeed, the pair distribution function and, therefore, also $S(q)$ are not very

sensitive to the large-distance behavior of the potential: as discussed, for instance, in Ref. 43, visibly different potentials may produce structures with essentially identical pair distribution functions. On the other hand, thermodynamic quantities are very sensitive to the tail of the potential, hence differ for models MHG and M1, even when a density-dependent corona diameter is used.

IV. STAR POLYMER PHASE DIAGRAM

Since star polymers interpolate between linear chains, which only have a fluid phase for all densities, and hard colloids, which have a fluid-solid transition, star polymers are expected to behave in both ways depending on f .^{9,44} For $f < f_c$ one expects only a fluid phase, while for $f > f_c$ a fluid and a solid phase are expected. In Refs. 9,44, f_c was estimated to be of order 100. In Ref. 18 a much more careful analysis was performed using model M1, finding $f_c \approx 34$. For $f_c < f \lesssim 60$ they found a small range of densities (note that $\Phi \approx 3.4\eta$, where η is the volume fraction defined in Ref. 18), $1.5 \lesssim \Phi \lesssim 2$, in which a solid bcc phase occurs, with reentrant melting as Φ increases. For larger values of f , the solid phase was more complex, with several crystalline states appearing at different densities. The presence of a solid phase for large values of f was later confirmed experimentally: Ref. 19 observed a solid bcc phase by using $f = 67$ starlike block copolymer

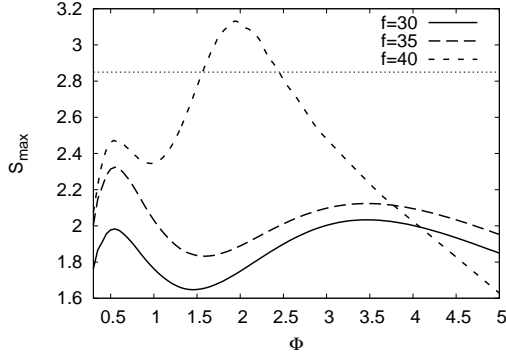


FIG. 7: Structure factor maximum $S_{\max} = \max S(q)$ as a function of Φ for $f = 30, 35, 40$. We use the MHG model and the RY closure.

micelles.

Since the thermodynamical properties of model M1 are quite different from those of model MHG, we wish now to check if and how the conclusions of Ref. 18 change when potential (2) is used. To determine the presence of a liquid-solid transition we use two different approximate methods. First, we use the Hansen-Verlet criterion:^{45,46} the phase transition occurs when the maximum S_{\max} of $S(q)$ exceeds 2.85. Second, we use the MHNC method^{34,36} and identify the phase transition by requiring $\eta_{HS} \approx 0.49$, where η_{HS} is the packing fraction of the reference hard-sphere model.

Since potential MHG has only been computed up to $f = 35$ and the region where the fluid-solid transition occurs corresponds to $f \gtrsim 30$, we have extended the MHG potential to $f = 40$. For this purpose we need to fix the five parameters that appear in Eq. (2). Parameter b_f is known,¹⁵ $b_f = 94.6$. Then, we note that a_f and d_f have a tiny dependence on f , hence it should be safe to use a simple extrapolation of the values appropriate to $f = 30$ and 35: $a_f = 1.78$, $d_f = 0.68$. Parameter τ_f is not precisely known and is approximately constant for $f \gtrsim 10$. We take $\tau_f = 0.5$. To fix c_f , we require the model to reproduce the second-virial combination A_2 : $A_2 \approx 41.96$ for $f = 40$.³¹ This gives $c_f = 84.2$.

In Fig. 7 we report the maximum S_{\max} of $S(q)$ for $f = 30, 35, 40$. For $\Phi < 5$, S_{\max} shows a nonmonotonic behavior with two maxima, one in the dilute region and one for $\Phi \gg 1$. For $f = 30$ and 35 the maximum S_{\max} is always smaller than 2.85, hence no fluid-solid transition is expected. For $\Phi = 40$ instead, S_{\max} is larger than 2.85 in the density range $1.6 \lesssim \Phi \lesssim 2.4$ (the maximum corresponds to $\Phi \approx 1.94$ with $S_{\max} = 3.13$). Hence, the Hansen-Verlet method allows us to infer that $35 < f_c \lesssim 40$. Moreover, the solid phase should appear at values of Φ close to 2, i.e. in a range of densities that is similar to that reported in Ref. 18.

The same analysis can be repeated by using the MHNC closure. In Fig. 8 we report η_{HS} as a function of Φ for

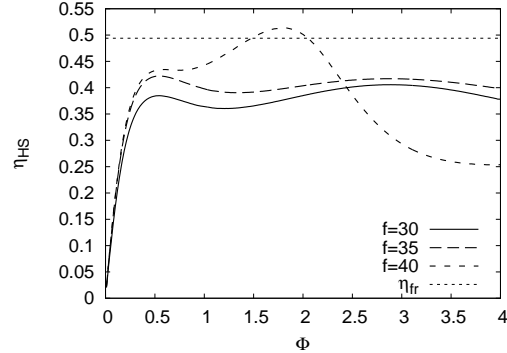


FIG. 8: Effective hard-sphere packing fraction η_{HS} determined by using the MHNC closure as a function of Φ . The horizontal line corresponds to the boundary of the fluid-solid coexistence $\eta_{HS} = 0.49$.

$f = 30, 35, 40$. For $f = 30, 35$ the effective hard-sphere packing fraction is always lower than 0.49, which gives the boundary of the fluid-solid coexistence line. For $f = 40$, instead it reaches a maximum $\eta_{HS} = 0.51$ for $\Phi = 1.81$. Hence, the MHNC analysis predicts crystallization in a small Φ interval that extends from $\Phi = 1.5$ to $\Phi = 2.0$.

The results of the two analyses are fully consistent and allow us to conclude with confidence that $35 < f_c \lesssim 40$. We therefore confirm the conclusions of Ref. 18, although we predict the fluid-solid transition to occur for slightly larger values of f (Ref. 18 predicted $f_c \approx 34$).

V. CONCLUSIONS

In this paper we investigate the thermodynamic behavior of three different CG models appropriate to describe dilute star-polymer solutions. Model MHG uses the exact pair potential, model M1, which should be applied for $f > 10$, is inspired by the Daoud-Cotton model, while model M2 is a phenomenological modification which shows a large-distance Gaussian behavior and which is expected to be realistic for $f \lesssim 10$. We find that model M2 provides a reasonable approximation to the thermodynamics and to the structure, even for $f > 10$. On the other hand, model M1 significantly underestimates the pressure and does not provide the correct structure factor. If one wishes to reconcile structural results for model M1 with those of model MHG, one might consider a density dependent corona diameter, as it is usually done in the analysis of the experimental data. However, while good agreement is obtained for the structure factor, model M1 with state-dependent interactions is completely inconsistent from a thermodynamic point of view: the compressibility factor shows an unphysical decrease as the density increases.

We investigate in detail the phase diagram of star poly-

mers by using model MHG. We use both the Hansen-Verlet criterion and the MHNC approximation to estimate the smallest value f_c of the functionality f for which a fluid-solid transition occurs. Both analyses are consistent with $35 < f_c \lesssim 40$. Our findings are in qualitative agreement with those of Ref. 18, which predicted $f_c \approx 34$ by using model M1, and with experiments, which ob-

served crystallization for $f \gtrsim 60$. Our data are also consistent with the presence of reentrant melting for f close to 40: the solid phase should be stable only in a small density interval centered around $\Phi \approx 1.8$ -1.9.

We thank Giuseppe D'Adamo for useful comments.

* Electronic address: Roberto.Menichetti@roma1.infn.it

† Electronic address: andrea.pelissetto@roma1.infn.it

¹ G. S. Grest, L. J. Fetters, J. S. Huang, and D. Richter, *Adv. Chem. Phys.*, vol. 94, I. Prigogine and S. A. Rice eds. (Wiley, NY, 1996) p. 67.

² D. Vlassopoulos, G. Fytas, T. Pakula, and J. Roovers, *J. Phys.: Condens. Matter* **13**, R855 (2001).

³ C. N. Likos, *Phys. Rep.* **348**, 267 (2001); *Soft Matter* **2**, 478 (2006).

⁴ C. von Ferber, A. Jusufi, C. N. Likos, H. Löwen, and M. Watzlawek, *Eur. Phys. J. E* **2**, 311 (2000).

⁵ P. G. Bolhuis, A. A. Louis, and J. P. Hansen, *Phys. Rev. E* **64**, 021801 (2001).

⁶ A. Pelissetto, *Phys. Rev. E* **85**, 021803 (2012).

⁷ C. N. Likos, H. Löwen, M. Watzlawek, B. Abbas, O. Jucknischke, J. Allgaier, and D. Richter, *Phys. Rev. Lett.* **80**, 4450 (1998).

⁸ M. Daoud and J. P. Cotton, *J. Phys. (Paris)* **43**, 531 (1982).

⁹ T. A. Witten and P. A. Pincus, *Macromolecules* **19**, 2509 (1986).

¹⁰ D. Richter, O. Jucknischke, L. Willner, L. J. Fetters, M. Lin, J. S. Huang, J. Roovers, C. Toporowski, and L.-L. Zhou, *J. Phys. (Paris) IV* **3**, C8-3 (1993).

¹¹ A. Jusufi, M. Watzlawek, and H. Löwen, *Macromolecules* **32**, 4470 (1999).

¹² A. M. Rubio and J. J. Freire, *Comp. Theor. Polym. Sci.* **10**, 89 (2000).

¹³ A. Jusufi, J. Dzubiella, C. N. Likos, C. von Ferber, and H. Löwen, *J. Phys: Condens. Matter* **13**, 6177 (2001).

¹⁴ B. Krüger, L. Schäfer, and A. Baumgartner, *J. Phys. (Paris)* **50**, 3191 (1989).

¹⁵ H.-P. Hsu and P. Grassberger, *Europhys. Lett.* **66**, 874 (2004).

¹⁶ C. Domb and G. S. Joyce, *J. Phys. C* **5**, 956 (1972); see also Ref. 28 for a precise determination of the optimal parameter.

¹⁷ M. Watzlawek, H. Löwen, and C. N. Likos, *J. Phys.: Condens. Matter* **10**, 8189 (1998).

¹⁸ M. Watzlawek, C. N. Likos, and H. Löwen, *Phys. Rev. Lett.* **82**, 5289 (1999).

¹⁹ M. Laurati, J. Stellbrink, R. Lund, L. Willner, D. Richter, and E. Zaccarelli, *Phys. Rev. Lett.* **94**, 195504 (2005).

²⁰ A. J. Archer, C. N. Likos, *J. Phys.: Condens. Matter* **14**, 12031 (2002).

²¹ J. Dzubiella, C. N. Likos, and H. Löwen, *J. Chem. Phys.* **116**, 9518 (2002).

²² M. Camargo and C. N. Likos, *Phys. Rev. Lett.* **104**, 078301 (2010).

²³ B. Lonetti, M. Camargo, J. Stellbrink, C. N. Likos, E.

Zaccarelli, L. Willner, P. Lindner, and D. Richter, *Phys. Rev. Lett.* **106**, 228301 (2011).

²⁴ G. Foffi, F. Sciortino, P. Tartaglia, E. Zaccarelli, F. Lo Verso, L. Reatto, K. A. Dawson, and C. N. Likos, *Phys. Rev. Lett.* **90**, 238301 (2003).

²⁵ F. Lo Verso, L. Reatto, G. Foffi, P. Tartaglia, and K. A. Dawson, *Phys. Rev. E* **70**, 061409 (2004).

²⁶ C. von Ferber, A. Jusufi, M. Watzlawek, C. N. Likos, and H. Löwen, *Phys. Rev. E* **62**, 6949 (2000).

²⁷ H.-P. Hsu, W. Nadler, and P. Grassberger, *Macromolecules* **37**, 4658 (2004).

²⁸ S. Caracciolo, B. M. Mognetti, and A. Pelissetto, *J. Chem. Phys.* **125**, 094903 (2006).

²⁹ S. Caracciolo, B. M. Mognetti, and A. Pelissetto, *Macromol. Theory Simul.* **17**, 67 (2008).

³⁰ L. Lue and S. B. Kiselev, *Int. J. Thermophys.* **23**, 117 (2002).

³¹ F. Randisi, MSc thesis, Sapienza Università di Roma, 2013.

³² T.-Y. Wang, C.-M. Fang, Y.-J. Sheng, and H.-K. Tsao, *J. Chem. Phys.* **130**, 124904 (2009).

³³ J. F. Douglas, J. Roovers, and K. F. Freed, *Macromolecules* **23**, 4168 (1990).

³⁴ J. P. Hansen and I. McDonald, *Theory of Simple Liquids*, 3rd ed. (Academic Press, Amsterdam, 2006)

³⁵ F. J. Rogers and D. A. Young, *Phys. Rev. A* **30**, 999 (1984).

³⁶ Y. Rosenfeld and N. W. Ashcroft, *Phys. Rev. A* **20**, 1208 (1979).

³⁷ L. Verlet and J. J. Weis, *Phys. Rev. A* **5**, 939 (1972).

³⁸ D. Henderson and E. W. Grundke, *J. Chem. Phys.* **63**, 601 (1975).

³⁹ F. Lado, *Phys. Lett. A* **89**, 196 (1982).

⁴⁰ This factorization is only valid for small Φ and small qR_g . For $\Phi \gtrsim 1$ large deviations are expected as soon as $qR_g \gtrsim 1$. A thorough discussion of several factorization formulae is presented in V. Krackoviak, J. P. Hansen, and A. A. Louis, *Europhys. Lett.* **58**, 53 (2002), together with an improved formula, obtained by using the polymer reference interacting site model (PRISM).

⁴¹ J. Stellbrink, J. Allgaier, M. Monkenbusch, D. Richter, A. Lang, C. N. Likos, M. Watzlawek, H. Löwen, G. Ehlers, and P. Schleger, *Progr. Colloid Polym. Sci.* **115**, 88 (2000).

⁴² A. A. Louis, *J. Phys.: Condens. Matter* **14**, 9187 (2002); G. D'Adamo, A. Pelissetto, and C. Pierleoni, [arXiv:1211.2694](https://arxiv.org/abs/1211.2694).

⁴³ F. Müller-Plathe, *Chem. Phys. Chem.* **3**, 754 (2002).

⁴⁴ T. A. Witten, P. A. Pincus, and M. E. Cates, *Europhys. Lett.* **2**, 137 (1986).

⁴⁵ J. P. Hansen and L. Verlet, *Phys. Rev.* **184**, 151 (1969).

⁴⁶ J. P. Hansen and D. Schiff, *Mol. Phys.* **25**, 1281 (1973).